Eur. Phys. J. D **27**, 125–130 (2003)
DOI: 10.1140/epjd/e2003-00232-4

THE EUROPEAN PHYSICAL JOURNAL D

Radial velocity profile reconstruction by Doppler spectroscopy measurements

A.L. Balandin[a], Y. Murata[b], and Y. Ono[c]

High Temperature Plasma Center, University of Tokyo, 2–11–16 Yayoi, Bunkyo–ku, Tokyo 113–8656, Japan

Received 16 October 2002 / Received in final form 24 January 2003
Published online 29 July 2003 –

Abstract. An inversion method for plasma velocity determination was developed under the assumption of axial symmetry of plasmas. The specific right-hand side of equation (9) allows one to use experimental data without the need of differentiation which causes substantial reconstruction errors. The problem was formulated in the vorticity approach, and then Helmholtz's decomposition theorem for vector fields was used. Numerical simulation results for the algorithm verification, and real experimental data were applied for determination of radial velocity distribution.

PACS. 07.05.Tp Computer modeling and simulation – 02.60.Cb Numerical simulation; solution of equations – 02.30.Zz Inverse Problems – 52.70.Kz Optical (ultraviolet, visible, infrared) measurements

1 Introduction

Plasma emits radiation over a broad frequency range. Characteristics of the radiation are related to plasma parameters then may be applied for diagnostics [1–4]. The methods of diagnostics using the radiation emitted by atoms and ions are based on the relationship between the line intensity and profile on the one hand and plasma parameters on the other. These methods are quite attractive since they do not introduce any perturbations into plasma. Though such diagnostics represent a major source of plasma information, the principal difficulty bound up with the application of these methods consists in the interpretation of the measured radiation characteristics. To obtain data on the spatial distribution of the radiation power, one usually measures the radiation intensity at different locations on the surface and along different paths, with subsequent solution of the integral Abel or Radon equations thus obtained [4–7]. In presence of plasma motion, however, neither Abel inversion nor scalar tomography methods may be used directly because the emission of any given wavelength depends on the orientation of the observation line [8,9]. This paper describes a method of 1-D tomography reconstruction for torus plasma diagnostics — mainly a visible light tomography which employs the plasma line spectrum. The numerical method for vector tomography has been developed to be applied to axial symmetry plasma measurements to extract the Doppler shift of spectral lines. Our merging device TS-3 can produce one or two spherical tokamaks of major radius of 0.2 m and aspect ratio of 1.2–1.9 inside its cylindrical vacuum chamber having the length of 0.99 m and the diameter of 0.75 m. The spectrum line emission of various impurity species was measured by detectors located outside the vacuum vessel.

In the first part of this paper, we intend to show how the vector tomography equation can be derived for spectroscopic measurements. Parts two and three describe the mathematical method for solving the vector tomography problem, computer simulations and computation of real experimental data. Under the restriction that $\mathbf{V}$ is divergenceless ($\mathsf{div}\,\mathbf{V} = 0$) in a bounded region, it is shown that the vector reconstruction problem is solved uniquely [11].

2 Inversion of Doppler spectroscopy data

Under the conditions that self-absorption and refraction may be neglected, the intensity of radiation from the plasma $I_{\boldsymbol{\xi}}(\nu';u)$ can be found simply by integrating the power emitted along the line of observation $L(u,\boldsymbol{\xi})$ (see Fig. 1) [8–10]:

$$I_{\boldsymbol{\xi}}(\nu';u) = \int\limits_{L(u,\boldsymbol{\xi})} \varepsilon(\nu';\mathbf{x},\boldsymbol{\eta})\,\mathrm{d}l = \int\limits_{\mathbf{R}^2} \varepsilon(\nu';\mathbf{x},\boldsymbol{\eta})\delta(u-\mathbf{x}\cdot\boldsymbol{\xi})\,\mathrm{d}\mathbf{x}, \qquad (1)$$

[a] e-mail: balandin@katsurai.t.u-tokyo.ac.jp
On leave from the Institute of System Dynamics and Control Theory, Irkutsk.
[b] e-mail: murata@katsurai.t.u-tokyo.ac.jp
[c] e-mail: ono@katsurai.t.u-tokyo.ac.jp

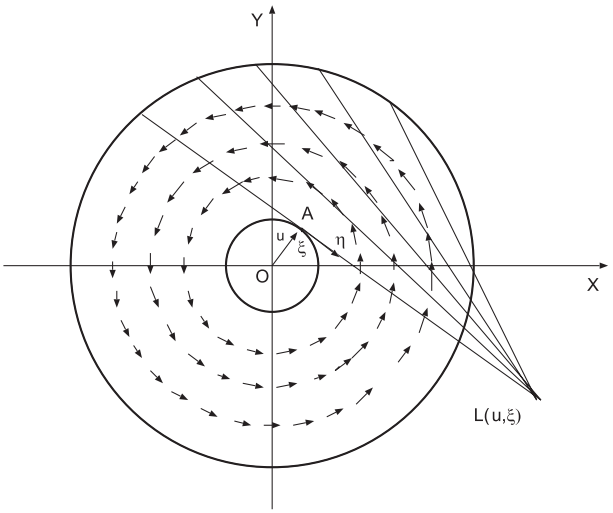

Fig. 1. The scheme of data registration in the spectroscopic experiment. The position of chord-lines of observation is defined by the vector $\boldsymbol{\xi}$ and by the distance $u = OA$, $\boldsymbol{\xi} \cdot \boldsymbol{\eta} = 0$.

where the unit vector $\boldsymbol{\xi}$ defines the position of line observation, and the unit vector $\boldsymbol{\eta}$ is directed along the observation line. The $\varepsilon(\nu'; \mathbf{x}, \boldsymbol{\eta})$ is the local emissivity profile. In special cases, when the particle velocity distribution is Maxwellian, the Doppler frequency shift results is a Gaussian line profile

$$\varepsilon(\nu'; \mathbf{x}, \boldsymbol{\eta}) = \frac{\varepsilon_0(\mathbf{x})}{\sqrt{2\pi}\Delta\nu'(\mathbf{x})} \exp\left(-(\nu' - \vartheta)^2 / 2\Delta\nu'^2\right), \quad (2)$$

where $\vartheta = \boldsymbol{\vartheta} \cdot \boldsymbol{\eta}$ is the normalized Doppler frequency shift of the spectral line, $\boldsymbol{\vartheta} = V(\mathbf{x})/c$ is the dimensionless velocity field, $\nu' = (\nu - \nu_0)/\nu_0$ is the normalized frequency, $\varepsilon_0(\mathbf{x})$ is isotropic emissivity, and $\Delta\nu'$ is the line width. Nonetheless, in the general case, the measured signal (1) along an observation line is not Gaussian and depends on the direction of observation at a given wavelength. Therefore, equation (1) cannot be directly inverted either by Abel's or by scalar tomography techniques [8]. However, some information can be obtained by integrating the spectral profile over the normalized frequency ν', thus introducing the spectral moments of the line–integrated emission by the formula [9]:

$$\mu^{(n)} = \int_{-\infty}^{\infty} I_{\boldsymbol{\xi}}(\nu'; u)\ \nu'^n \mathrm{d}\nu'. \quad (3)$$

The first moment is defined by the velocity distribution and by the direction of line of observation

$$\mu^{(1)} = \int_{L(u,\boldsymbol{\xi})} \varepsilon_0(\mathbf{x})\ \boldsymbol{\vartheta}(\mathbf{x}) \cdot \mathrm{d}\mathbf{l} \equiv \mathcal{V}\{\varepsilon_0 \boldsymbol{\vartheta}\}(u, \boldsymbol{\eta}), \quad (4)$$

where vector $\mathrm{d}\mathbf{l}$ is directed along the observation line, $\boldsymbol{\eta}$, and $\mathcal{V}$ is a vector Radon transform, which is defined as follows:

$$\mathcal{V}\{\boldsymbol{\vartheta}\}(u, \boldsymbol{\eta}) = \int_{L(u,\boldsymbol{\xi})} \boldsymbol{\vartheta}(\mathbf{x}) \cdot \mathrm{d}\mathbf{l}. \quad (5)$$

The zero moment is a usual Radon transform of the emissivity distribution defined by

$$\mu^{(0)} = \int_{L(u,\boldsymbol{\xi})} \varepsilon_0(\mathbf{x}) \mathrm{d}l \equiv \mathcal{R}\{\varepsilon_0\}(u, \boldsymbol{\xi}). \quad (6)$$

Equation (4) is related to the tomography of vector fields and requires special inversion methods. First of all, let us consider an inversion of the equation (5). For measurements in some two-dimensional space the unit vector $\boldsymbol{\xi}$ is given by $\boldsymbol{\xi} = (\cos\theta, \sin\theta)$, where θ is the angle between the positive direction X-axis and the line OA. The inversion problem in this case can be considered in terms of the vorticity vector function $\boldsymbol{\zeta} = \mathsf{curl}\,\boldsymbol{\vartheta}$, which has only one component $\boldsymbol{\zeta} = (0, 0, \zeta)$. By using the Helmholtz's decomposition theorem [12]

$$\boldsymbol{\vartheta} = \mathsf{curl}\,\boldsymbol{\Psi} + \mathsf{grad}\,\Phi, \quad (7)$$

and some properties of Radon transform [13], the following result is obtained

$$\mathcal{V}\{\boldsymbol{\vartheta}\}(u, \boldsymbol{\eta}) = -\frac{\partial}{\partial u}\mathcal{R}\{\psi\}(u, \boldsymbol{\eta}). \quad (8)$$

Since $\boldsymbol{\vartheta}$ is confined to the $x-y$-plane, a single component of the vector potential $\boldsymbol{\Psi}$ in the z-direction exists; *i.e.* one may write $\boldsymbol{\Psi} = \psi \boldsymbol{e}_z$. The equation (8) may be rewritten in the equivalent form

$$\mathcal{R}\{\psi\}(u, \boldsymbol{\eta}) = -\int_{-\infty}^{u} \mathcal{V}\{\boldsymbol{\vartheta}\}(u', \boldsymbol{\eta}) \mathrm{d}u'. \quad (9)$$

The details for the deduction of formula (9) can be found in [10]. If we are given spectroscopic measurement data, the moments $\mu^{(1)} = \mathcal{V}\{\varepsilon_0 \boldsymbol{\vartheta}\}(u, \boldsymbol{\eta})$ and $\mu^{(0)} = \mathcal{R}\{\varepsilon_0\}(u, \boldsymbol{\eta})$ can be obtained, and an inversion of the vector Radon transform may be reduced to a scalar Radon inversion of the following measured data:

$$\mathcal{R}\{\psi\}(u, \boldsymbol{\eta}) = -\int_{-\infty}^{u} \mu^{(1)}(u', \boldsymbol{\eta}) \mathrm{d}u'. \quad (10)$$

Any algorithm of scalar tomography can now be applied for determination of the ψ-function. Equation (10) shows that only the solenoidal component ψ (and hence, $\mathsf{curl}\,\boldsymbol{\Psi}$) is determined uniquely from the line–integrated data. There is no contribution from the irrotational component $\mathsf{grad}\,\Phi$ into equation (10). In the case of axial symmetry of plasmas there is no dependence on the unit vector $\boldsymbol{\eta}$ in equation (10), and the operator of Radon transformation $\mathcal{R}$ can now be replaced with the operator of Abel's transformation. Equation (10) will have the following form:

$$\mathcal{A}\{\psi\}(u) = -\int_{-\infty}^{u} \mu^{(1)}(u') \mathrm{d}u', \quad (11)$$

and the potential function ψ, as well-known, can now be written as follows (see Appendix B):

$$\psi(r) = \frac{1}{\pi} \int_r^R \frac{\mu^{(1)}(u)\,\mathrm{d}u}{(u^2 - r^2)^{1/2}}. \tag{12}$$

From the computational viewpoint, formula (12) is very convenient because it does not require differentiation of experimental data. It is well-known that differentiation procedure of noised data is unstable, and special regularization techniques are usually needed. Integral (12) can be computed by many different ways (see, for instance, [1], p. 185), but the simplest method used for our computer simulation is given in Appendix B. Assuming now that only the solenoidal component of motion is present, the velocity components are defined as follows:

$$\vartheta_x = \frac{1}{\varepsilon_0}\frac{\partial\psi}{\partial r}\frac{y}{r}, \quad \vartheta_y = -\frac{1}{\varepsilon_0}\frac{\partial\psi}{\partial r}\frac{x}{r}, \quad |\boldsymbol{\vartheta}| = \frac{1}{\varepsilon_0}\frac{\partial\psi}{\partial r}. \tag{13}$$

The function ε_0 is obtained as a result of inversion of equation (6) under the assumption of axial symmetry.

3 Computer simulation and experimental data analysis

In this section, the results of computer simulation are given for demonstration of the algorithm. The real experimental data are also used for velocity profiles reconstruction. Owing to the model of velocity distribution we have examined the algorithm using the scheme of measurements as shown in Figure 1. The total number of measurements for 8 chords (that corresponds to real experimental scheme) is used in the numerical experiments. Two exact velocity profiles write

$$\vartheta = \exp\left(-((r-0.6)/0.3)^2\right) \begin{cases} \sin(3\,\pi\, r) \\ \cos(3.5\,\pi\, r) \end{cases}$$

and their reconstructions are given in Figure 2. The reconstruction was performed with the data spoilt by some artificial noise. The noise level was taken to be 2.5% of the maximum level of measured emission amplitude (spectroscopic data). The error of reconstruction depending on the number of chord integrals is represented in Figure 3. The discrepancy between exact and reconstructed models is calculated by the formula:

$$\Delta^2 = \frac{\sum\limits_{i=0}^{M} \left(|\vartheta_i| - |\tilde{\vartheta}_i|\right)^2}{\sum\limits_{i=0}^{M} \vartheta_i^2},$$

where summation is performed over all grid points, $|\vartheta_i|$ and $|\tilde{\vartheta}_i|$ are the values for the model and its reconstruction at the ith node of the grid. One can observe that the increase of the number of ray-sums over 15 does not reduce the error of reconstruction anymore. This effect is caused by the numerical scheme, noise level and by the complexity of the model employed.

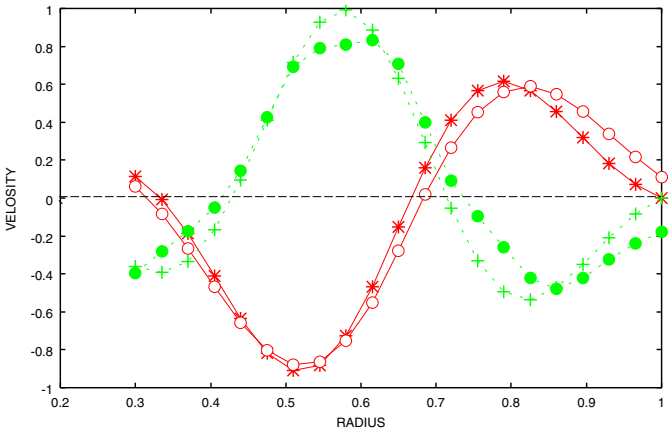

Fig. 2. Radial velocity profiles (dimensionless) for the first exact model ($\cdots+\cdots$) and ($\cdots\bullet\cdots$) its reconstruction, as well as for the second exact model ($-*-$) and ($-\circ-$) its reconstruction. Relative errors of reconstruction are 3.27% and 4.71% for the first and second models, respectively.

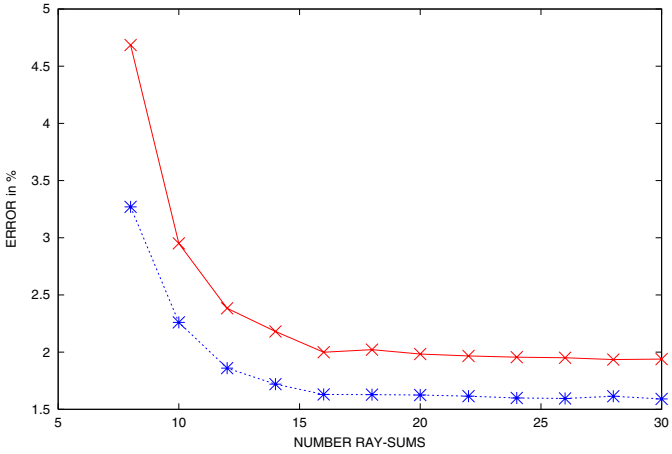

Fig. 3. Error of reconstruction (in per cent) depending on the number of chord measurements for the first model ($\cdots*\cdots$) and ($-\times-$) for the second one, respectively.

In our experiment, eight chord measurements are performed for two merging counter helicity plasma toroids. It was reported that the two spheromaks with oppositely directed toroidal fields caused the dynamic magnetic reconnection to drive the inner and outer toroidal flow with opposite polarity [15]. The chord profiles against normalized frequency are plotted in Figure 4. The green, red and blue profiles correspond to the measurements at three different time moments: 180 μs, 193 μs and 200 μs, respectively. The poloidal flux contours measured by internal probes are shown in Figure 5. The velocity profiles calculated by using the chord measurements are shown in Figure 6. The normalized radius $r = 0.19$ corresponds to the radius of the central coils, $R = 65$ mm, and $r = 1.0$ corresponds to the device radius, $R = 340$ mm.

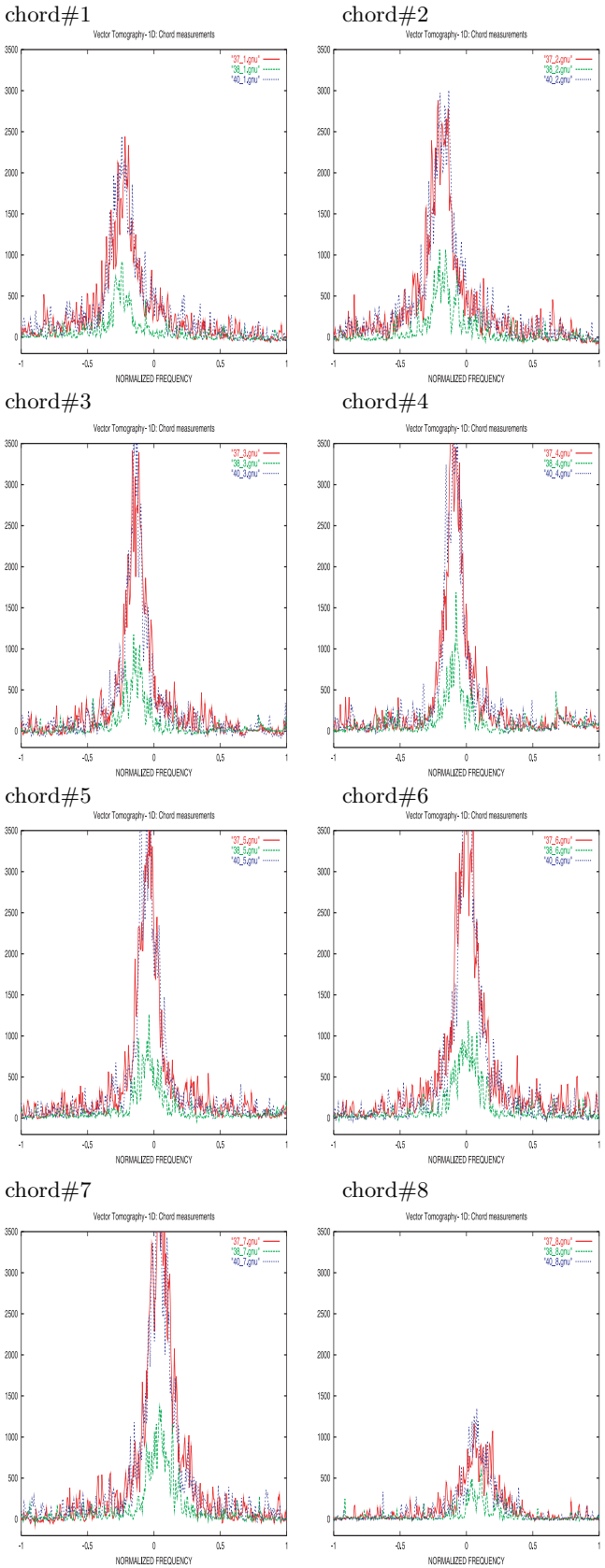

Fig. 4. Eight chord-line spectrum measurements at three different time moments of plasma evolution: 180 μs, before (green) the reconnection, 193 μs, at the time (red) and 200 μs, after it (blue).

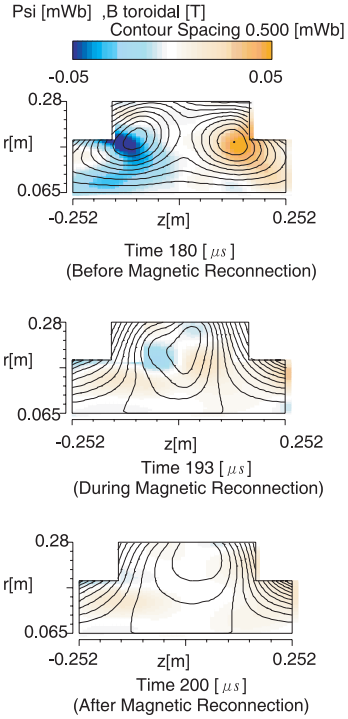

Fig. 5. Poloidal flux contours before plasma merging, 180 μs, at the time of reconnection, 193 μs and after it, 200 μs.

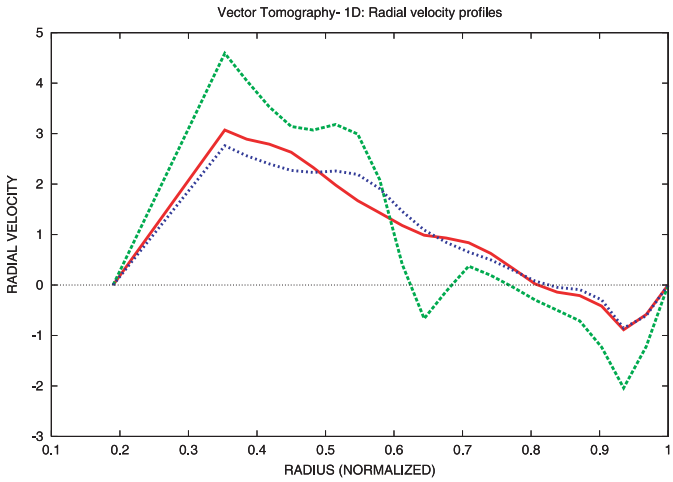

Fig. 6. Radial velocity profiles (dimensionless) at three different time moments: 180 μs (green), 193 μs (red) and 200 μs (blue).

The renormalization dimensional coefficient for transforming the relative value of velocity distribution $\vartheta(r)$ to the absolute value of $V(r)$ is given by the formula $K = c\,\delta\nu/(\delta\nu'\,\nu_0)$, that is, $V(r) = K\,\vartheta(r)$, where $\delta\nu = 0.0128$ Å in our experiment, $\delta\nu' = 0.035$ is the dimensionless frequency step size in our computations, $\nu_0 = 4861$ Å is the frequency of the observation line, and c is the speed of light.

4 Conclusion

The numerical method for reconstructing the radial profile of plasma velocity has been described. The method has been developed by applying the vector Radon transform to spectroscopic measurement data. The components of the vector field have been recovered by differentiation of a single component of the vector potential (stream function). For the vector potential, ψ, reconstruction technique based on Abel inversion formula has been used. It should be noted, though, that the accuracy of the profile determination by this technique is substantially dependent on the number of chord measurements and on the actual profile shape. The integral nature of the initial data masks thin sharp changes if they exist in ψ, and therefore, in $\boldsymbol{\vartheta}$ over the profile. We cannot evaluate the exact effect introduced by data errors into the computation of the velocity distribution, but it is possible state that contribution error is not larger than in the corresponding numerical experiments.

The first author would like to express his gratitude to the staff of High–Temperature Plasma Center, University of Tokyo, for their great hospitality.

Appendix A

A.1 The vector Radon transform

If $\boldsymbol{\vartheta} \in \mathcal{L}(\mathbf{R^2}, \mathbf{R^2})$, then vector $\mathcal{V}$- and scalar $\mathcal{R}$-Radon transforms are related to each other by the following

$$\frac{\partial}{\partial u}\mathcal{V}\{\boldsymbol{\vartheta}\}(u,\boldsymbol{\eta}) = \mathcal{R}\{\zeta\}(u,\boldsymbol{\eta}), \tag{14}$$

Proof.
Firstly, rewrite the left-hand side of (14) to the equivalent form:

$$\frac{\partial}{\partial u}\mathcal{V}\left\{\boldsymbol{\vartheta}\right\}(u,\boldsymbol{\eta}) = \frac{\partial}{\partial u}\mathcal{R}\left\{\boldsymbol{\vartheta}\cdot\boldsymbol{\eta}^{\perp}\right\}(u,\boldsymbol{\eta}). \tag{15}$$

Taking the Fourier transform of the right side and using the central slice theorem [14], one obtains

$$\mathcal{F}_1^{-1}\left\{\frac{\partial}{\partial u}\mathcal{R}\left\{\boldsymbol{\vartheta}\cdot\boldsymbol{\eta}^{\perp}\right\}\right\}(\sigma,\boldsymbol{\eta}) =$$

$$\mathrm{i}\sigma(2\pi)^{1/2}\mathcal{F}_2^{-1}\{-\vartheta_1\eta_2+\vartheta_2\eta_1\}(\sigma\boldsymbol{\vartheta})$$

$$= (2\pi)^{1/2}(-\mathrm{i}\sigma\eta_2\mathcal{F}_2^{-1}\{\vartheta_1\}(\sigma\boldsymbol{\vartheta}) + \mathrm{i}\sigma\eta_1\mathcal{F}_2^{-1}\{\vartheta_2\}(\sigma\boldsymbol{\vartheta})$$

$$= (2\pi)^{1/2}\left(-\mathcal{F}_2^{-1}\left\{\frac{\partial\vartheta_1}{\partial x_2}\right\}(\sigma\boldsymbol{\vartheta}) + \mathcal{F}_2^{-1}\left\{\frac{\partial\vartheta_2}{\partial x_1}\right\}(\sigma\boldsymbol{\vartheta})\right)$$

$$= (2\pi)^{1/2}\mathcal{F}_2^{-1}\{\zeta\}(\sigma\boldsymbol{\vartheta}) = \mathcal{F}_1^{-1}\mathcal{R}\{\zeta\}(\boldsymbol{\vartheta},\sigma),$$

where the symbols $\mathcal{F}_2^{-1}$ and $\mathcal{F}_1^{-1}$ denote two- and one-dimensional direct Fourier transforms, respectively. The inverse Fourier transform gives the formula (14).

Appendix B

B.1 Evaluation of the equation (11)

Direct and inverse Abel transforms are as follows

$$g(u) \equiv \mathcal{A}\{f\}(u) = 2\int_u^R \frac{f(r)\,r\,\mathrm{d}r}{(r^2-u^2)^{1/2}}$$

$$f(r) \equiv \mathcal{A}^{-1}\{g\}(r) = -\frac{1}{\pi}\int_r^R \frac{g'(u)\,\mathrm{d}u}{(u^2-r^2)^{1/2}}. \tag{16}$$

Applying (16) to (10) we obtain the following relation

$$\psi(r) = \frac{1}{\pi}\int_r^R \frac{\mu^{(1)}(u)\,\mathrm{d}u}{(u^2-r^2)^{1/2}},$$

$$\psi(r_j) = \frac{1}{\pi}\sum_{i=j}^{N}\int_{r_i}^{r_{i+1}} \frac{\mu^{(1)}(u)\,\mathrm{d}u}{(u^2-r_j^2)^{1/2}}, \tag{17}$$

where $j = 1\cdots N$, the grid $\{r_j\}$ is given with the constant step size Δr along the radial coordinate. Under the assumption that $\mu^{(1)}(u)$ is sufficiently smooth within the grid step interval Δr, the equation (17) is rewritten as follows

$$\psi(r_j) \approx \frac{1}{\pi}\sum_{i=j}^{N}\mu^{(1)}(u_i)\int_{r_i}^{r_{i+1}} \frac{\mathrm{d}u}{(u^2-r_j^2)^{1/2}}$$

$$= \frac{1}{\pi}\sum_{i=j}^{N}\mu^{(1)}(u_i)\,I_{ij},$$

where the internal integral I_{ij} is

$$I_{ij} = \ln\left[\frac{r_{i+1}\left(1+\sqrt{1-r_j^2/r_{i+1}^2}\right)}{r_i\left(1+\sqrt{1-r_j^2/r_i^2}\right)}\right].$$

References

1. *Plasma Diagnostics*, edited by W. Lochte-Holtgreven (American Institute of Physics, New York, 1995)
2. R.W.P. McWhirter, *Plasma Diagnostic Techniques* (Academic Press, New York, 1965)
3. W.L. Wiese, in *Plasma Diagnostic Techniques* (Academic Press, New York, 1965)
4. E.I. Kuznetsov, D.A. Shcheglov, *High Temperature Plasma Diagnostic* (Atomizdat, Moscow, 1980) (in Russian)
5. Y.I. Ostrovskii, M.M. Butusov, G.V. Ostrovskaya *Holographic Interferometry* (Nauka, Moscow, 1977)

6. C.D. Maldonado, A.P. Caron, H.N. Olsen, J. Opt. Soc. Am. **55**, 1247 (1965)
7. C.D. Maldonado, H.N. Olsen, J. Opt. Soc. Am. **56**, 1305 (1966)
8. R.E. Bell, Rev. Sci. Instrum. **68**, 1273 (1997)
9. J. Howard, Plasma Phys. Control. Fusion **38**, 489 (1996)
10. A.L. Balandin, Y. Ono, Eur. Phys. J. D **17**, 337 (2001)
11. S.J. Norton, Geophys. J. **97**, 161 (1988)
12. P.M. Morse, H. Feshbach, *Methods of Theoretical Physics* (McGraw-Hill, New York, 1953)
13. S.R. Deans, *The Radon transform and some of its applications* (John Wiley & Sons, New-York, 1983)
14. F. Natterer, *The Mathematics of Computerized Tomography* (John Wiley & Sons Ltd and B.G. Teubner, Stuttgart, 1986)
15. Y. Ono *et al.*, Phys. Rev. Lett. **76**, 3328 (1996)